Hydration Properties of Extruded Starch Foams and Films

Denis Lourdin, Laurent Chaunier, Guy Della Valle, Kamal Kansou, Jean-eudes Maigret, Paul Minaret, Emma Poupard, Killian Robion

Starch - Stärke

WILEY-VCH
Starch

RESEARCH ARTICLE OPEN ACCESS

Hydration Properties of Extruded Starch Foams and Films

Denis Lourdin | Laurent Chaunier | Guy Della Valle | Kamal Kansou | Jean-Eudes Maigret | Paul Minaret | Emma Poupard | Killian Robion

Biopolymers, Interactions & Assemblies (BIA) UR 1268, INRAE, Nantes, France

Correspondence: Denis Lourdin (denis.lourdin@inrae.fr)

Received: 7 July 2025 | **Revised:** 16 January 2026 | **Accepted:** 3 February 2026

ABSTRACT

The study focuses on hydration during immersion of extruded starch foams and thermomoulded starch films. A collection of starch foam samples from 1% to 70% amylose (99%–30% amylopectin) processed under various extrusion conditions has been used. The alveolar structures of foams are characterized by various densities (from 98 to 465 kg/m^3), cell size, and median cell wall thickness. The kinetics of water uptake are measured and fitted by using the Peleg model. It is shown that the larger the size of the alveoli and the thinner the walls, the greater the water uptake, whatever the amylose–amylopectin composition of the walls. The water uptake of films is controlled by the thickness of films (from 0.25 to 1 mm) and the amylose-amylopectin composition, with a threshold value of amylose content between 40% and 50%.

1 | Introduction

Extruded starch is widely used or studied for non-food applications such as pharmaceutical tablets, controlled release systems, and degradable biomaterials [1–7]. For these applications, starch may simply be a filler, or it may play an active role, for instance by modulating the release of an active ingredient. For all these applications, the functionality is achieved by immersing the starch-based system in an aqueous medium. These materials are often used in the form of dense materials, but starch foams can also be interesting. For example, starch foams have recently been studied as biomaterials that supply glucose in the presence of enzyme amyloglucosidase [8]. Hydration during immersion is the first stage mechanism that governs the release properties of glucose during enzymatic hydrolysis. In spite of its interest, no study has been performed on the mechanisms of water absorption of starch extruded foam. This lack might be explained by the focus on using these materials as an alternative to expanded polystyrene, and hence reducing their water sensitivity [9]. However, the hydration of solid starch-rich foams (i.e., cereal flour) is a well-known issue in foods like, for instance, ready-to-eat breakfast cereals [10]. These products are generally consumed when immersed in milk, and during the immersion, they undergo rehydration and, sometimes, undesirable changes in texture. The kinetics of extruded breakfast cereal moisture uptake during storage or soaking have been studied [11–13] as well as the kinetics of textural changes [14]. For example, the moisture uptake of extruded cereal mixture, based on 70% starch, was measured from 300% to 650% with densities from 85 to 130 kg/m^3 [14, 15]. To describe water absorption in grains or food products during storage or soaking, various mathematical relations, such as Weibull or Peleg models, are used [11]. They enable the forecasting of water uptake with time in porous food products. These two models have been used by Mathieu et al. in order to fit experimental water uptake kinetics during soaking of bread crumb for 1 h [16]. This study highlighted the strong influence of the density of cell connectivity, cell and wall width distributions. The kinetics of water sorption can also be described by the relation of Peppas based on physical mechanisms of diffusion of small molecules in a polymer matrix [17].

The present study proposes to focus on hydration during immersion of extruded starch foams and films. Starch foams are formed at the extrusion outlet by the growth of vapor bubbles in a

Abbreviations: DSC, Differential Scanning Calorimetry; MCS, Mean Cell Size; MCWT, Mean Cell Wall Thickness; TGA, ThermoGravimetric Analysis; WAI, Water Absorption Index (WAI).

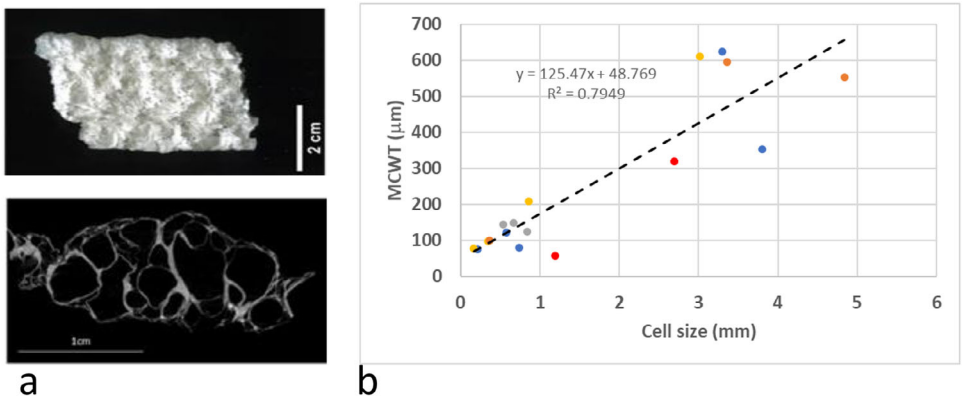

FIGURE 1 | (a) extruded foam (photograph at the top) and alveolar structure determined by tomography (2D slice presented at the bottom); (b) Mean cell wall thickness as a function of cell size of foams, determined by x-ray tomography, foam A (●); foam B1 (●); foam B2 (●); foam C (●).

viscous fluid that solidifies during cooling. These are alveolar solid materials constituted by cells and walls. In addition to density, size, and thickness distribution, respectively, characterize the macroscopic structure of starch foams. The composition of the wall material depends on the type of starch used. The specific feature of such biopolymer foams is that the hydration involves two mechanisms: the filling of the alveoli, which generally occupy more than two-thirds of the foam volume (i.e., porosity), and the swelling of the walls, made of amorphous starch, which is highly hydrophilic. Particular attention will be paid to the effect of density, foam cellular structure, and amylose/amylopectin ratio for the films. For this purpose, a collection of starch foam samples of different compositions and processed under various extrusion conditions has been used.

2 | Materials and Methods

2.1 | Samples Elaboration and Cellular Structure Characterization

The samples were produced by extrusion following the method given by Della Valle et al. [18]. Two corn starches from the Roquette Company (Lestrem, France) were used: amylomaize Eurylon (A), theoretically containing 70% amylose; and waxy maize (D), containing 99% amylopectin. The amylose content of amylomaize was previously determined at 72% +/− 2%. Three intermediate compositions (B1, B2, and C) were produced by mixing starches A and D. Extrusion was achieved on a Clextral BC45 twin-screw extruder (Firminy, France) (screw diameter: 56 mm; screw length: 1 m) provided with a rheometric slit die, under various controlled conditions: temperature, added water, feed rate and screw rotation speed. No plasticizer other than water has been used to produce the materials. The different conditions (water content and Specific Mechanical Energy) used for the process allow for obtaining various foam structures and densities.

Cell wall thickness and cell size values were determined by x-ray tomography. The tomography images were acquired with a Skyscan 1174 device (Bruker-axs, Karlsruhe, Germany). The sample was inserted into a sponge block attached to the goniometer so that the flow axis of the die was vertical (Figure 1). Analysis of the 3D images reconstructed from the scans provides information about the cells and walls of the alveolar structure. Median values of cell wall thickness and cell size were obtained using the method of granulometry by openings. The principle of this method is to apply a series of openings of a structural element (such as a 3×3×3 voxel cube, for example) of increasing width, followed by a sieving of the objects of the image. The voxels eliminated are then counted at each stage and represented in the form of a curve of granulometric distribution of walls or cells from which the median values are derived [19]. Voxel size ranges between 6.5 and 19 µm.

2.2 | Thermomoulding

Thin and thick films were produced by thermomoulding powder from ground extrudates. The extruded samples were ground, hydrated to reach a water content of 20%, and the mixture was homogenized with a pestle. A hydraulic press was used with molds in the form of discs with 20-mm diameter holes for three different thicknesses (0.2, 0.5, and 1 mm). The hydrated powder was placed in each hole of the plate previously placed on a Teflon sheet. A second Teflon sheet was placed on top of the samples, and the whole setup was introduced between the two heating plates of the press. Each heating plate was heated to 120°C and the sample was subjected to a pressure of 200 bars for 10 min. The thickness of disc-shaped samples was accurately measured with a caliper.

2.3 | Amylose Content Analysis

The determination of amylose by differential scanning calorimetry (DSC) is based on the complexation properties of amylose with fatty acids and was achieved using the method described by Mestres et al. [20]. DSC measurements were performed with a DSC Q100 from TA Instruments (New Castle, USA). In a high-pressure stainless-steel DSC capsule, 50 µL of a 4% LPC (L-a-lysophosphatidylcholine) solution was added to 5 mg of sample. The reference capsule contained 50 µL of water. The capsules were then subjected to the following cycle: (1) 10°C/min to 130°C; (2) isothermal at 130°C for 2 min; (3) 3°C/min to 20°C; and (4) isothermal at 20°C for 2 min. This cycle was repeated twice. The uncertainty of the amylose content measurement was +/− 2%.

2.4 | Water Content by TGA

Moisture content of initial (or "dry") foams was determined by thermogravimetric analysis, performed on a TA 2050 Thermogravimetric analyser from TA Instruments (New Castle, USA). The sample is heated to 120°C and held at this temperature for 120 min to ensure that all the water in the sample has evaporated. The water content of the sample can be determined from the mass loss observed on the thermogram, corresponding to the initial water content of the sample.

2.5 | Density Measurements

The bulk density of the sample d_{sample} is calculated by weighing a quantity M_{sample}, of foam and by measuring its volume through the displacement of glass beads (bulk density d_{beads}, diameter 3 mm). First, a non-deformable container is filled with a quantity of glass beads. Next, the foam is immersed in the glass beads, and the excluded beads are weighed. If M_{beads} is the mass of beads excluded on the introduction of foam, the bulk density of the extrudates is:

$$d_{sample}\ (kg/m3) = d_{beads}\ \frac{M_{sample}}{M_{beads}}$$

From density measurements, porosity is determined by the following relation:

$$Porosity\ (\%) = \frac{d_{solid} - d_{sample}}{d_{solid}} \times 100$$

where d_{solid} is the solid density of starch extruded foams and equals 1400 $kg.m^{-3}$.

2.6 | Hydration During Immersion

Extruded foam samples of approximate size 10 × 10 mm were cut in the extrudate flat ribbon, whose thickness varies from 3 to 10 mm, depending on the composition. For the thermomoulded samples, the experiment is performed on the entire disc-shaped sample. After careful weighing, samples were immersed in a glass container filled with distilled water at 20°C and covered with a lid to prevent them from floating. Then, at regular intervals, they are taken out of the water. A part of the water remaining at the surface of the sample was carefully removed by paper wiping, and the sample was weighed using a 0.1 mg analytical balance. The experiment was repeated at different times. To improve reproducibility, each experiment was repeated on three samples. The water uptake during immersion was calculated according to the following relation:

$$Water\ uptake\,(\%) = \frac{M_t - M_{init}}{M_{init}} \times 100$$

where: M_t is the mass of the sample at time t of immersion, M_{init} is the mass of the sample before immersion.

Results are presented with error bars representing the deviations from the mean of the three replicas.

The experimental data of water uptake have been fitted by using the Peleg model, commonly used for modelling water absorption in various grains and foods (dense or expanded) during soaking:

$$M\,(t) = \frac{t}{K_1 + K_2 t}$$

where M (%) is the water uptake at time t, on a dry basis, K_1 is the Peleg rate constant ($\%.min^{-1}$), and K_2 is the Peleg capacity constant (%).

2.7 | Mechanical Properties Under Immersion

Foam's mechanical properties were measured in large deformations by the uniaxial compression test. A universal tension/compression testing machine (Adamel Lhomargy, Type DY-34B, France) equipped with a parallel plates geometry (∅ = 20 mm) was used to compress foams' cylindrical samples (∅ = 23 mm) at a constant compression speed set at 10 mm/min. The measure has been carried out on samples in their initial state (dry) and at different times of immersion in water (2, 10, 20, 60 min) at ambient temperature. After immersion, the sample is removed from the bath and drained slightly before the compression test. The measurements realized on three replicas at each time of immersion are sample-consuming, and the quantity available was insufficient to measure hydration and mechanical properties on the same samples. Therefore, mechanical properties were measured on samples distinct from those on which hydration properties have been determined. However, the samples panel chosen for mechanical properties is representative of compositions A–D, with densities close to those of the samples studied for their hydration properties.

3 | Results and Discussion

3.1 | Composition and Structure of Foams

Extruded foams have a rectangular section (Figure 1). Their structure characteristics, density, and porosity are reported in Table 1. Samples are named A, B1, B2, C, and D according to their amylose content determined respectively at 72, 50, 39, 21, 1%, ±2%. Water content is comprised between 6.5% and 11% before hydration. The different extrusion conditions, differentiated by the number appearing after the sample name, resulted in a wide range of densities from 98 to 465 kg/m^3 as measured by the bead displacement method. Their alveolar structure is characterized by cell size and median cell wall thickness, determined by x-ray tomography (Figure 1a), as also reported in Table 1. Figure 1b shows the variations of mean cell wall thickness with cell size, which are fairly correlated, whatever the foam density. This result, already observed by Babin et al. [19], suggests that cell wall thickness increases with air cell size, hence leading to a coarser structure [21].

3.2 | Kinetics of Foams Hydration

Sample hydration has been carried out on all foam samples. Samples C.2 and D disintegrated during immersion, which means

TABLE 1 | Foams composition, structure, and Peleg coefficient.

Sample	Moisture content(%)	Amylose content(%)	Cell size(mm)	Median cell wall thickness(μm)	Density (kg/m^3)	Porosity (%)	$1/K_1$ ($\%.min^{-1}$)	$1/K_2$(%)
A.1	8.1	74.2	0.74	80	144	90	172 ± 2	337 ±
A.2	9.1	**74.3**	3.8	353	109	92	1102 ± 1040	564 ± 40
A.3	9.3	69.9	0.579	121	296	79	106 ± 110	194 ± 28
A.5	8.8	72.1	3.3	624	244	83	150 ± 152	175 ± 58
A.6	9.2	72.4	0.22	75	327	77	66	70
B1.1	9.3	51	2.69	319	118	92	554 ± 732	300 ± 66
B1.2	9.5	49	1.192	**56**	**98**	**93**	539 ± 392	502 ± 149
B2.1	9.4	39.7	0.67	147	269	81	131 ± 52	191 ± 4
B2.2	10.1	38.7	0.54	143	359	**74**	51 ± 6	145 ± 31
B2.4	9.6	40.9	0.84	123	267	81	83 ± 34	265 ± 35
B2.5	8.7	40.4	ND	ND	219	84	103 ± 29	382 ± 40
C.1	**11.0**	21	0.86	208	**465**	67	103 ± 81	128 ± 17
C.2	7.6	19.2	3.02	**611**	274	80	Nd	Nd
C.3	9.0	20.6	0.35	98	329	77	139 ± 166	160 ± 64
C.4	10.2	23.1	**0.167**	78	325	77	358 ± 203	122 ± 14
D.1	**6.5**	1.3	**4.84**	553	262	81	Nd	Nd
D.2	10.8	**0.4**	0.368	100	367	**74**	Nd	Nd
D.3	9.5	0.9	3.36	595	339	76	Nd	Nd

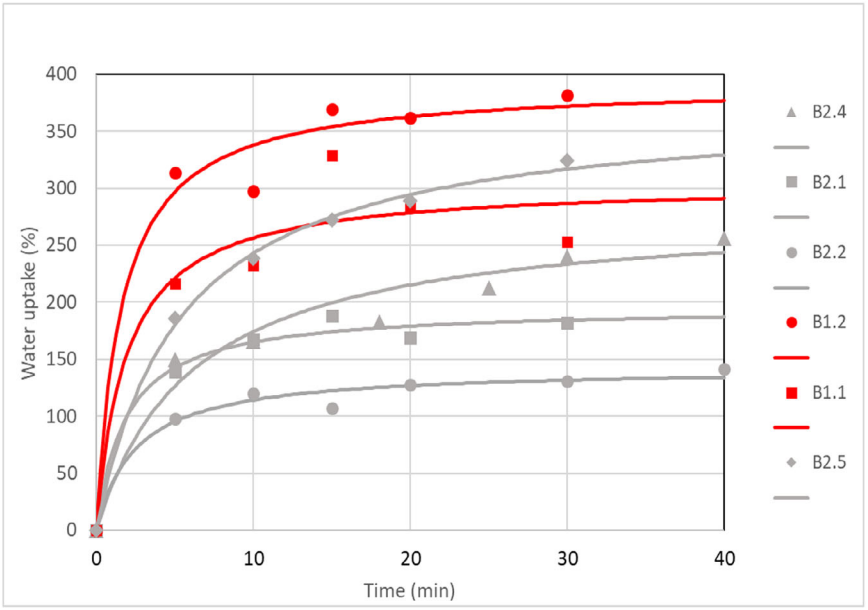

FIGURE 2 | Examples of hydration kinetics of samples B1 (red) and B2 (grey) extruded under different conditions. Continuous lines represent fitting by the Peleg model ($R^2 > 0.88$).

that the hydration measurements cannot be validated. These behavior points can be attributed to their high amylopectin content. For all other samples, the kinetics of hydration during immersion followed a monotonous increasing trend. Figure 2 shows the results obtained on one of the three repetitions for the B1 and B2 samples. The water uptake stabilizes after 30–40 min, and its values extend over a large interval, from 130% to 380%, depending on foam structure. These large values underline the water absorption capacity of these foams, which can be explained by the filling of the air cells and the swelling of the cell walls.

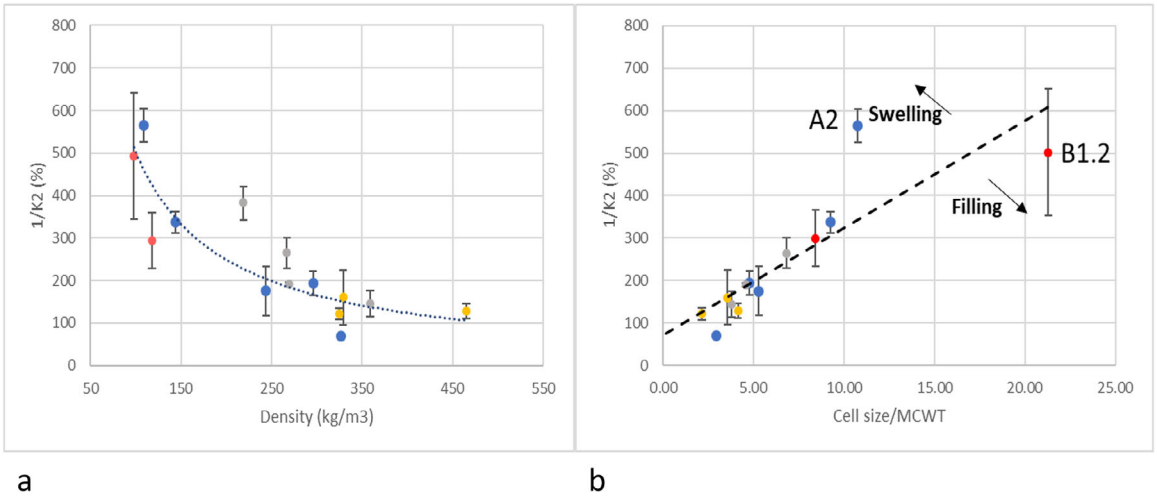

FIGURE 3 | Evolution of water uptake (1/K2) with density fitted with a power function ($y = 53006\ x^{-1.012}$, $R^2 = 0.7118$) (a) and with the cell size reported to the mean cell wall thickness (MCS/MCWT) fitted with a linear function ($y = 25.142x + 72.765$, $R^2 = 0.7318$) (b). foam A (●); foam B1 (●); foam B2 (●); foam C (●).

The K_1 and K_2 have been calculated for each repetition of experiments by using the Peleg model described previously. The average values of $1/K_1$ and $1/K_2$ and the standard deviation are reported in Table 1. Due to the difficulty of the measurements in the first minutes of hydration, there is very high variability in the rate constant $1/K_1$. The quantity $1/K_2$ is the water uptake when the imbibition time tends toward infinity (%) and corresponds to the global water retention of the starch foams. To examine the relation between hydration and the structure of foams, the variations of $1/K_2$ are represented with density in Figure 3a. The rapid decrease of $1/K_2$ with density can be fitted by a power function. As shown by the various colors in the figure, there is no correlation between $1/K_2$ and amylose content of foams. By using the power function 1/K2 = f(density), the theoretical water uptake of a dense material, that is, which does not contain any cell, for a density of 1400 kg/m^3, can be calculated, leading to a value of 33%. The evolution of $1/K_2$ is also represented with the ratio of mean cell size reported to the mean cell wall thickness (= MCS/MCWT) (Figure 3c). This ratio is equivalent to the ratio of the volume of air cells to the volume of solid walls, for closed foams. The positive linear correlation suggests that: (1) water uptake mechanisms depend mainly on structural factors on a macroscopic scale, that is, foam cells and walls, (2) the larger the size of the alveoli and the thinner the walls, the greater the water uptake, whatever the amylose-amylopectin composition of the walls. Considering that MCS/MCWT represents the ratio of the volume to be filled to the volume to be swollen by water, the trend featured by the regression line may indicate how each mechanism contributes to foam hydrating: larger cell size value favors the filling of cells (bottom region), whereas larger wall thickness value would induce an increased contribution of starch swelling (upper region). This suggestion can be supplemented by examining the two foams B1.2 and A.2, which have similar final water uptake (1/K2 = 500%) (see Figure 3b). The foam B1.2 with the highest MCS/MCWT ratio (below this trend) should owe its water uptake to the filling of its pore network, rather than to the swelling of cell walls. For the foam A.2 (above this trend), the final water uptake would come more from the swelling of cell walls than the filling of pores.

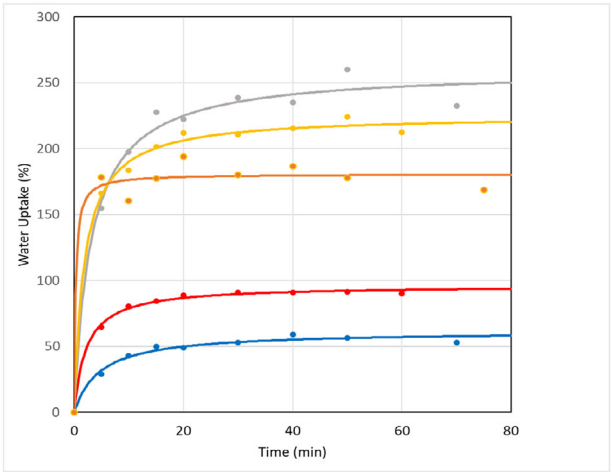

FIGURE 4 | Hydration kinetics for films of a thickness of 0.25 mm, representative of each group of amylose content: film A (●); film B1 (●); film B2 (●); film C (●); film D (●).

3.3 | Kinetics of Film Hydration

3.3.1 | Effect of Amylose Content

Films with various thicknesses have been produced from ground foams by thermomoulding. Their molecular composition (amylose/amylopectin) reported in Table 2 is identical to that of the foams from which they are derived (Table 1). The kinetics of hydration during immersion have been measured on all films listed in the table. Figure 4 shows the increase in water content with time for five films selected as representative of different amylose content with a thickness of 0.25 mm. The trends of curves are quite similar for all samples, with a rapid increase during the first 20 min and a stabilization at a value that greatly depends on amylose content. The data from the collection of samples has been fitted by using the Peleg relation. The resulting values of coefficient $1/K_1$ and $1/K_2$ are reported in Table 2. Values of $1/K_2$ vary between 50% and 280%. They are lower than those of the

TABLE 2 | Films composition, Peleg, and diffusion coefficients.

	Films thickness	0.25 mm		0.5 mm		1 mm			
Sample	Amylose content(%)	$1/K_1$ (%min^{-1})	$1/K_2$(%)	$1/K_1$ (%min^{-1})	$1/K_2$(%)	$1/K_1$ (%min^{-1})	$1/K_2$(%)	Diffusion coef(m^2. s^{-1})	SD
A.1*	74.2	32 ± 5	87 ± 9	10 ± 5	80 ± 18	2.4 ± 0.3	25 ± 1	9,1E-12	1,7E-12
A.2	74.3	12 ± 3	60 ± 2					5,3E-12	1,6E-12
A.3	69.9	9 ± 4	56 ± 3					4,5E-12	1,1E-12
A.5	72.1	19 ± 5	54 ± 1					8,8E-12	1,9E-12
A.6	72.4	ND	ND					ND	ND
B1.1	51	53 ± 9	96 ± 2					1,3E-11	1,7E-12
B1.2	49	155 ± 150	137 ± 12					1,6E-11	8,3E-12
B2.1	39.7	91 ± 15	277 ± 15	11 ± 1	149 ± 16	5 ± 2	74 ± 10	8,8E-12	1,5E-12
B2.2	38.7	86 ± 5	268 ± 9					8,2E-12	2,7E-13
B2.4	40.9	64 ± 9	235 ± 13					6,9E-12	1,2E-12
B2.5	40.4	415 ± 463	203 ± 23					2,5E-11	1,7E-11
C.1	21	347 ± 416	237 ± 21					1,8E-11	1,5E-11
C.2	19.2	934 ± 69	235 ± 1	25 ± 10	121 ± 6	25 ± 10	65 ± 8	ND	ND
C.3	20.6	259 ± 169	208 ± 16					2,1E-11	1,0E-11
C.4	23.1	661 ± 3	206					ND	ND
D.1	1.3	557 ± 288	215 ± 44	183 ± 258	115 ± 2	46 ± 20	56 ± 4	3,5E-11	2,6E-11
D.2	0.4	615 ± 307	203 ± 17					4,3E-11	1,8E-11
D.3	0.9	ND	ND					ND	ND

*Additional data are available for thickness 0.19 and 0.6 mm give $1/K_2$ respectively at 76±8 and 50±2.

water absorption index (WAI) from 478% to 757% measured on corn starch extruded in various conditions of water, ground, and sieved at 250 µm [22]. This difference can be explained by the larger specific surface area of particles compared with films.

Figure 5 shows the evolution of $1/K_2$ for films of thickness 0.25 mm. This graph suggests that there is a threshold value of amylose content between 40% and 50%, below which $1/K_2$ is about 150% to 280%, whereas beyond this value, $1/K_2$ decreases to values between 130% and 50%. A threshold on hydration properties could be due to a phase separation between amylose-amylopectin, which has been observed many times in water diluted system [23, 24] with a phase inversion around an amylose/amylopectin ratio of 15/85 [25]. Leloup et al. reported also a phase inversion between 26% and 40% amylose on gel system between a state with a dispersed amylose phase in a continuous amylopectin matrix for lower amylose content, and vice versa for high amylose content. [26]. On solid films, Rindlav et al. reported a critical amylose proportion between 8% and 25%, from a phase-separated system to a more homogeneous system with a continuous amylose network as the amylose proportion increases [27]. The same explanation can be inferred for the films of extruded starch: for higher amylose content, amylopectin would be embedded in a continuous amylose phase. Since, after phase separation, amylose tends to be more crystalline than amylopectin, as shown by Myillarinen et al. [28], such films would therefore have a lower hydration rate.

3.4 | Determination of Diffusion Coefficient of Water in Films

In order to determine the kinetics of water penetration, the coefficient of water diffusion in the film, D, has been determined using the Peppas relation, which is a solution derived from Fick's second law:

$$\frac{M_t}{M_\infty} = 1 - \sum_{n=0}^{\infty} \frac{8}{(2n+1)^2 \pi^2} exp\left[\frac{-D\left((2n+1)^2 \pi^2\right)}{l} t\right]$$

It assumes a constant diffusion coefficient D in the x direction for a typical sorption experiment of a slab of a hydrophilic polymer of thickness l. Mt is defined as the mass of water uptake at time t, and M_∞ is the mass of water uptake as time approaches infinity [17].

The values of the diffusion coefficient calculated are reported in Table 2 for all films with a thickness of 0.25 mm. A decreasing trend from 4.10^{-11} to 4.10^{-12} m^2 s^{-1} appears when increasing amylose from 1 to about 74% amylose. The values are of the same order of magnitude as the values published by Thérien-Aubin. et al. for-amylose tablets: $D = 2.10^{-11}$ m^2 s^{-1} [2]. As expected, these values are lower than those found by Chevigny et al. for extruded starch containing 20% glycerol, around 10^{-10} m^2 s^{-1},

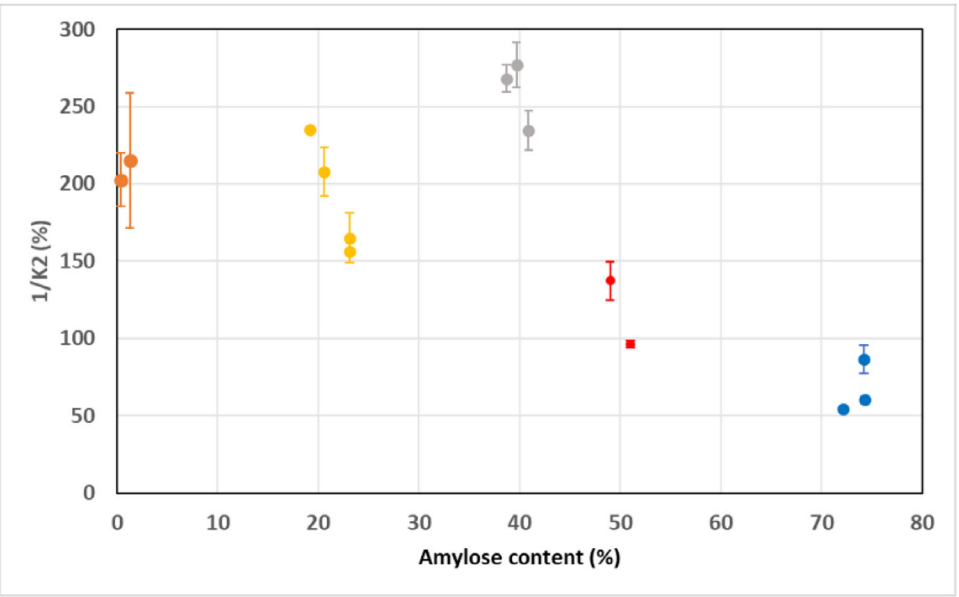

FIGURE 5 | Hydration rate (1/K2) for films of a thickness 0.25 mm with various amylose content: films A (●); films B1 (●); films B2 (●); films C (●); films D (●).

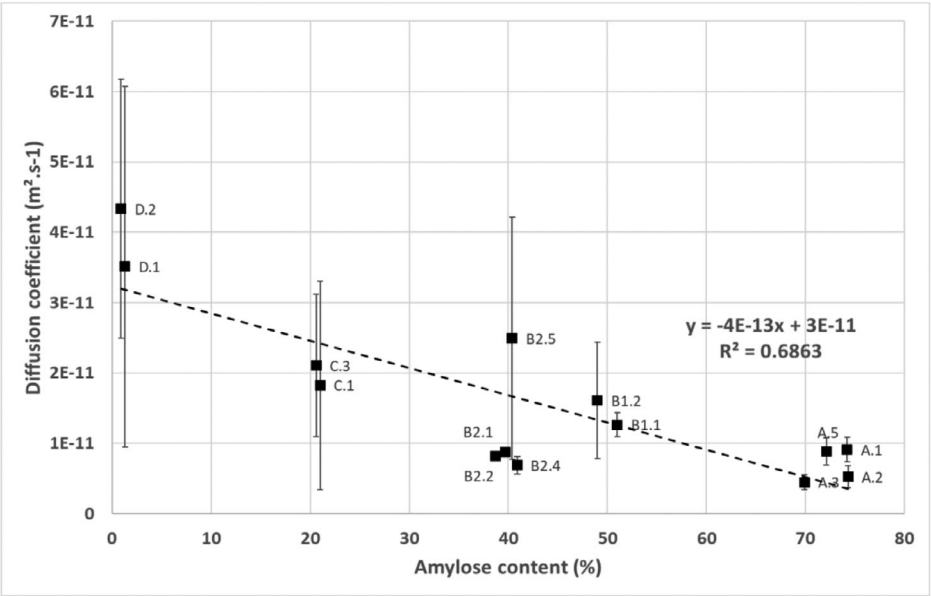

FIGURE 6 | Diffusion coefficient with amylose content in thermomoulded films.

since water mobility is likely larger in this latter material, due to the presence of the plasticizer [29]. Figure 6 shows that, despite large error bars, the decreasing trend can be fitted by a linear function. This result could be explained by the fact that, following a transformation combining the effects of water and temperature, amylose is known to reorganize more rapidly than amylopectin [30]. Consequently, in the films, water diffusion could be reduced in amylose-rich compositions by a crystalline network.

3.4.1 | Effect of Film Thickness

Figure 7 shows the evolution of water uptake (1/K2) with thickness determined for films A, B2, C, and D. For each amylose content, the data points decrease with film thickness following a logarithmic trend, whose equation is supplied on the graph. For all films, we observe a decrease of $1/K_2$ when the thickness increases by a factor of 4, from 0.25 to 1 mm. For the group of low amylose content (B2, C, and D), the quantitative decrease of water uptake (from 200%–280% to 50%–80%) is higher than for the amylose-rich film (A) (from 85%–90% to 25%). Finally, the values seem to be converging toward values close to 25%–75% water uptake for film thickness of about 1 mm, which agrees with previous studies conducted on extruded starch [1, 7]. These values are also in agreement with the value of 33% calculated previously for a non-expanded material from the results on foam hydration. On the left part of the figure, the trend curves show a significant increase in water uptake for low film thicknesses of the group of low amylose content (B2, C, and D).

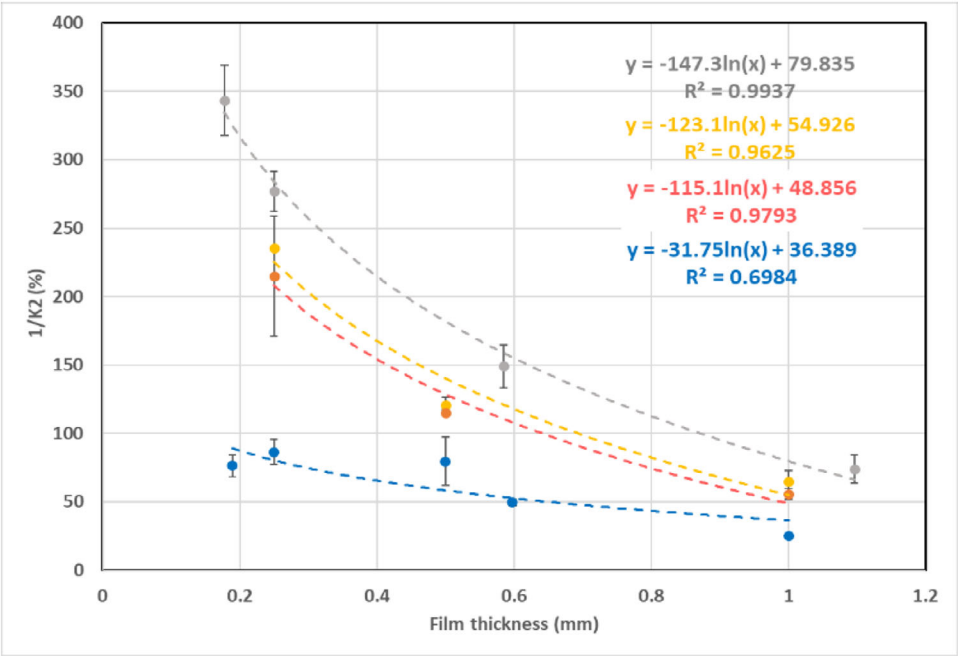

FIGURE 7 | Evolution of hydration rate (1/K2) with thickness of films with various amylose content: films A.1(●); films B2.1 (●); films C.2 (●); films D.1 (●).

TABLE 3 | Foams composition and density.

Sample	Amylose content(%)	Density(kg/m3)
A.2	74.3	109
B2.6	39	170
C.5	20	180
A.5	72.1	244
A.7	69	290
D.4	0.5	370
C.6	21	380

3.5 | Mechanical Properties During Hydration

The mechanical properties of foam samples have been measured at different times of immersion in water. The amylose content with respect to the four groups A, B2, C, and D, and the density of the samples studied are indicated in Table 3. For C.5 foam, it was only possible to measure the mechanical properties in the dry state because the sample dispersed within the first few seconds of immersion. For all other samples, whatever their origin or immersion time, all hydrated foams displayed the same mechanical behavior characterized, after a first step, by a linear stress increase from which the modulus was derived, before a stress plateau, indicating a threshold value, beyond which stress started to decrease, indicating sample softening or collapse (Figure 8a). In addition, the values of modulus (E) and threshold stress (σc) were highly correlated (Figure 8b). Both results suggest that the variations of stress with strain are governed by the same mechanisms, independently of the amylose level, always identified by the same color code in Figure 8b.

The variations of threshold stress for different immersion times are represented with the initial density (of dry foams) in Figure 9a. Mechanical properties are found to rank according to the density of the sample in agreement with the results obtained by Babin et al. on similar materials [19]. As expected, the stress decreases with immersion time, likely due to the hydration of the walls, which softens the material, a trend that seems independent of the amylose content of the starch material. To check this hypothesis, the stress values are normalized by dividing their numerical value by the value of the stress for initial (dry) foam, and the water uptake is calculated using the Peleg equation, whose coefficients have been determined in the preceding section (Table 1). For samples A.7, B2.6, and C.6, whose hydration properties were not determined, the coefficient values of samples A.3, B2.5, and C.3, respectively, with the same amylose content and similar density values, were used. The resulting variations (Figure 9b) underline the influence of water on the normalized threshold stress, as shown by the fair correlation between σ_r and water uptake (%). The dispersion may be attributed to the uncertainty in determining the water increase.

4 | Conclusion

The hydration kinetics of foams and films can be described by the Peleg model. However, the initial stages are difficult to capture, which leads to significant variability in the 1/K1 constants of the foams. The water uptake mechanisms of foams were found to depend mainly on structural factors on a macroscopic scale, density, and cellular structure: the larger the size of the alveoli and the thinner the walls, the greater the water uptake, whatever the amylose-amylopectin composition of the walls. Conversely, the water absorption of films is governed by the composition of the starch and the thickness of the films. In terms of composition, two distinct behaviors were observed, with water uptake two

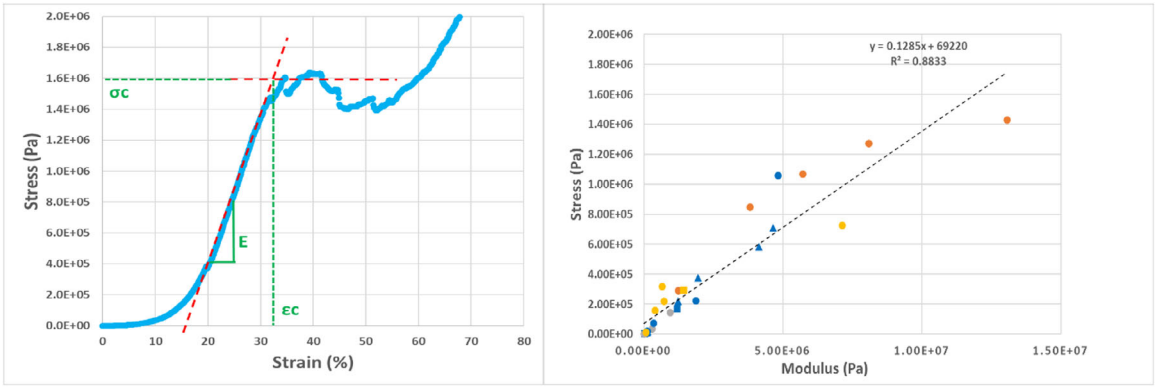

FIGURE 8 | Typical stress/strain curve obtained for hydrated foams (after t = 2 mn immersion) with retrieved mechanical properties (a) and variations of threshold stress with modulus (b) A.2 (■); A.5(▲); A.7 (●);B2.6 (●); C.6 (●); D.4 (●).

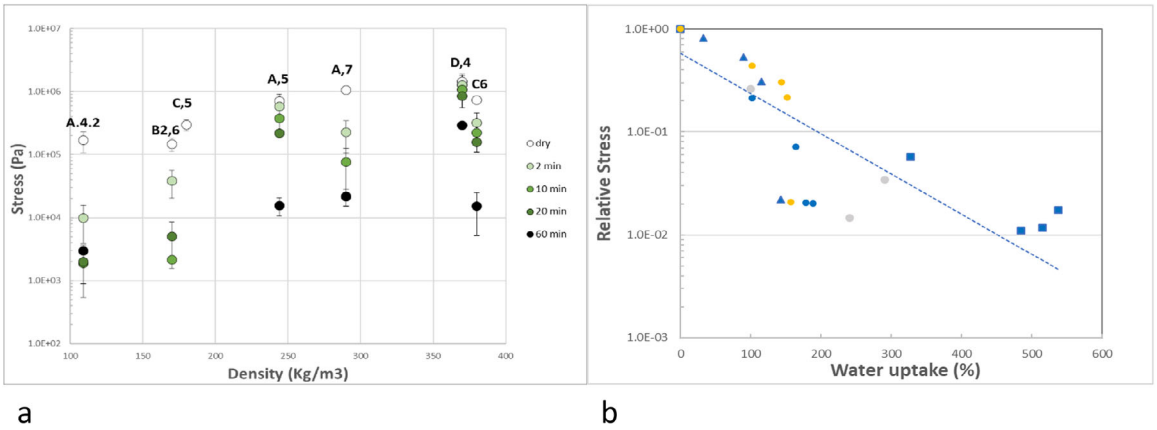

FIGURE 9 | Variations of threshold stress of hydrated foams: A.2 (■) ; A.5(▲) ; A.7 (●);B2.6 (●); C.6 (●); D.4 (●); (a) real values with density of dry foams for different immersion time; (b) normalized values with water increase for samples; dotted line represents best fit ($\sigma_r = 0.58\ \exp[-9.10^{-3} *$ Water uptake]; $r^2 = 0.6$).

to three times higher when amylopectin is the major phase rather than amylose. An increase in relative water absorption was observed with decreasing thickness, regardless of the starch composition. The swelling of the films can be described by a diffusion phenomenon, quantified by a D coefficient. Comparison of foam and film properties suggested that the filling of the foam cells is a more important mechanism in water absorption than the swelling of the cell walls. Finally, the mechanical properties of the hydrated foams are governed by their density (or porosity) and water content. These results concerning the hydration of starch materials may have an impact on all the applications, either food or non-food, where starchy foams are implemented.

Author Contributions

All the authors contributed to the investigation. Methodology: Denis Lourdin, Laurent Chaunier, Guy Della Valle, Kamal Kansou. Funding acquisition: Denis Lourdin. Writing – original draft: Denis Lourdin, Laurent Chaunier, Guy Della Valle, Kamal Kansou, and Killian Robion. Writing – review and editing: Denis Lourdin.

Acknowledgments

This work was funded by the French National Research Agency (ANR20-CE19-0002-02).

Open access publication funding provided by COUPERIN CY26.

Conflicts of Interest

The authors declare no conflicts of interest.

Data Availability Statement

The data that support the findings of this study are aAuthor: Please check funding information and confirm its correctness.vailable on request from the corresponding author. The data are not publicly available due to privacy or ethical restrictions.

References

1. A. Beilvert, F. Chaubet, L. Chaunier, et al., "Shape-memory Starch for Resorbable Biomedical Devices," *Carbohydrate Polymers* 99 (2014): 242–248.

2. H. Thérien-Aubin, W. E. Baille, X. X. Zhu, and R. H. Marchessault, "Imaging of High-Amylose Starch Tablets. 3. Initial Diffusion and Temperature Effects," *Biomacromolecules* 6 (2005): 3367–3372.

3. H. Therien-Aubin, X. X. Zhu, F. Ravenelle, and R. H. Marchessault, "Membrane Formation and Drug Loading Effects in High Amylose Starch Tablets Studied by NMR Imaging," *Biomacromolecules* 9 (2008): 1248–1254.

4. F. Ravenelle, R. H. Marchessault, A. Légaré, and M. D. Buschmann, "Mechanical Properties and Structure of Swollen Crosslinked High Amylose Starch Tablets," *Carbohydrate Polymers* 47 (2002): 259–266.

5. C. Freire, F. Podczeck, F. Veiga, and J. Sousa, "Starch-based Coatings for Colon-specific Delivery. Part II: Physicochemical Properties and In Vitro Drug Release from High Amylose Maize Starch Films," *European Journal of Pharmaceutics and Biopharmaceutics* 72 (2009): 587–594.

6. T. Kipping, R. Trindade, and H. Rein, "The Use of Hot-Melt Extruded Corn Starch Matrices as Drug Carrier Systems: A Thermophysical Characterization," *Starch—Stärke* 66 (2014): 923–933.

7. D. Velasquez, G. Pavon-Djavid, L. Chaunier, A. Meddahi-Pellé, and D. Lourdin, "Effect of Crystallinity and Plasticizer on Mechanical Properties and Tissue Integration of Starch-based Materials from Two Botanical Origins," *Carbohydrate Polymers* 124 (2015): 180–187.

8. A. Lescher, K. Kansou, G. Della Valle, H. Petite, and D. Lourdin, "Evaluation of Extruded Starch Foam for Glucose-Supplying Biomaterials," *Carbohydrate Polymers* 340 (2024): 122319.

9. M. A. Dircio-Morales, H. A. Fonseca-Florido, G. Velazquez, and C. A. Ávila-Orta, "Relationship among Extrusion Conditions, Cell Morphology, and Properties of Starch-Based Foams—A Review," *Starch—Stärke* 75 (2022): 2200103.

10. T. Lucas, D. Le Ray, and F. Mariette, "Kinetics of Water Absorption and Solute Leaching during Soaking of Breakfast Cereals," *Journal of Food Engineering* 80 (2007): 377–384.

11. M. Peleg, "An Empirical Model for the Description of Moisture Sorption Curves," *Journal of Food Science* 53 (1988): 1216–1217.

12. M. D. Machado, F. A. R. Oliveira, V. Gekas, and R. P. Singh, "Kinetics of Moisture Uptake and Soluble-solids Loss by Puffed Breakfast Cereals Immersed in Water," *International Journal of Food Science and Technology* 33 (1998): 225–237.

13. M. F. Machado, F. A. R. Oliveira, and L. M. Cunha, "Effect of Milk Fat and Total Solids Concentration on the Kinetics of Moisture Uptake by Ready-to-Eat Breakfast Cereal," *International Journal of Food Science and Technology* 34 (1999): 47–57.

14. G. Sacchetti, P. Pittia, M. Biserni, G. G. Pinnavaia, and M. D. Rosa, "Kinetic Modelling of Textural Changes in Ready-to-eat Breakfast Cereals During Soaking in Semi-skimmed Milk," *International Journal of Food Science and Technology* 38 (2003): 135–143.

15. G. Sacchetti, P. Pittia, and G. G. Pinnavaia, "The Effect of Extrusion Temperature and Drying-tempering on both the Kinetics of Hydration and the Textural Changes in Extruded Ready-to-Eat Breakfast Cereals During Soaking in Semi-Skimmed Milk," *International Journal of Food Science and Technology* 40 (2005): 655–663.

16. V. Mathieu, A.-F. Monnet, S. Jourdren, M. Panouillé, C. Chappard, and I. Souchon, "Kinetics of Bread Crumb Hydration as Related to Porous Microstructure," *Food & Function* 7 (2016): 3577–3589.

17. N. A. Peppas and L. Brannon-Peppas, "Water Diffusion and Sorption in Amorphous Macromolecular Systems and Foods," *Journal of Food Engineering* 22 (1994): 189–210.

18. G. DellaValle, B. Vergnes, P. Colonna, and A. Patria, "Relations Between Rheological Properties of Molten Starches and Their Expansion Behaviour in Extrusion," *Journal of Food Engineering* 31 (1997): 277–295.

19. P. Babin, G. Della Valle, R. Dendievel, D. Lourdin, and L. Salvo, "X-ray Tomography Study of the Cellular Structure of Extruded Starches and Its Relations with Expansion Phenomenon and Foam Mechanical Properties," *Carbohydrate Polymers* 68 (2007): 329–340.

20. C. Mestres, F. Matencio, B. Pons, M. Yajid, and G. Fliedel, "A Rapid Method for the Determination of Amylose Content by Using Differential-Scanning Calorimetry," *Starch—Stärke* 48 (1996): 2–6.

21. M. Kristiawan, L. Chaunier, G. Della Valle, A. Ndiaye, and B. Vergnes, "Modeling of Starchy Melts Expansion by Extrusion," *Trends in Food Science & Technology* 48 (2016): 13–26.

22. M. H. Gomez and J. M. Aguilera, "A Physicochemical Model for Extrusion of Corn Starch," *Journal of Food Science* 49 (1984): 40–43.

23. K. Svegmark and A. M. Hermansson, "Distribution of Amylose and Amylopectin in Potato Starch Pastes—Effects of Heating and Shearing," *Food Structure* 10 (1991): 117–129.

24. S. G. Ring, P. Colonna, K. J. I'Anson, et al., "The Gelation and Crystallisation of Amylopectin," *Carbohydrate Research* 162 (1987): 277–293.

25. J. L. Doublier and G. Llamas, eds. Dickinson, E., Walstra, P.in "Food Colloids and Polymers" (Woodhead Publishing, 2005): 138–146.

26. V. M. Leloup, P. Colonna, and A. Buleon, "Influence of Amylose-amylopectin Ratio on Gel Properties," *Journal of Cereal Science* 13 (1991): 1–13.

27. Å. Rindlav-Westling, M. Stading, and P. Gatenholm, "Crystallinity and Morphology in Films of Starch, Amylose and Amylopectin Blends," *Biomacromolecules* 3 (2002): 84–91.

28. P. Myllärinen, A. Buleon, R. Lahtinen, and P. Forssell, "The Crystallinity of Amylose and Amylopectin Films," *Carbohydrate Polymers* 48 (2002): 41–48.

29. C. Chevigny, L. Chaunier, R. Ferbus, P. Roblin, C. Rondeau-Mouro, and D. Lourdin, "In-Situ Quantitative and Multiscale Structural Study of Starch-Based Biomaterials Immersed in Water," *Biomacromolecules* 19 (2018): 838–848.

30. J. L. Putaux, A. Buléon, and H. Chanzy, "Network Formation in Dilute Amylose and Amylopectin Studied by TEM," *Macromolecules* 33 (2000): 6416–6422.